

Nanocrystal-Powered Nanomotor

B. C. Regan,^{†,‡,§} S. Aloni,^{†,‡} K. Jensen,^{†,‡} R. O. Ritchie,^{‡,||} and A. Zettl^{*,†,‡,§}

Department of Physics, Center of Integrated Nanomechanical Systems, and Department of Materials Science and Engineering, University of California, Berkeley, California 94720, and Materials Sciences Division, Lawrence Berkeley National Laboratory, Berkeley, California 94720

Received June 7, 2005; Revised Manuscript Received July 5, 2005

ABSTRACT

We have constructed and operated a nanoscale linear motor powered by a single metal nanocrystal ram sandwiched between mechanical lever arms. Low-level electrical voltages applied to the carbon nanotube lever arms cause the nanocrystal to grow or shrink in a controlled manner. The length of the ram is adjustable from 0 to more than 150 nm, with extension speeds exceeding 1900 nm/s. The thermodynamic principles governing motor operation resemble those driving frost heave, a natural solid-state linear motor.

The introduction of the steam engine in the industrial revolution marked the advent of useful mechanical systems powered by linear motors. Today linear motors using gas or liquid working fluids drive such important technologies as the internal combustion engine. Recent progress in the extreme miniaturization of electronic^{1,2} and mechanical³ systems raises the following question: can inorganic linear motors be fabricated and operated at the molecular or nanoscale level? Here we report the construction and operation of a synthetic nanoscale linear motor, driven by a single solid-state metal nanocrystal ram. The ram length and extension/retraction rates are controlled via low voltage electrical signals applied to mechanical lever arms contacting the ram.

In our implementation the entire nanomotor is composed of only two chemical species, one constituting the nanocrystal ram and its associated working matter storage reservoir and the other constituting the lever arms that couple the motor to its surroundings. As shown in Figure 1, a metal nanocrystal ram is sandwiched between two mechanical lever arms formed from multiwalled carbon nanotubes (MWNTs). Another metal nanocrystal, located on one of the lever arms near the ram, serves as the working matter reservoir. This “atom reservoir” sources metal atoms for ram extension and sinks metal atoms for ram contraction. Atom transfer between the reservoir and ram is controlled by an electrical current through the lever arms and the ram nanocrystal between them. The motor operates by growing and shrinking the nanocrystal ram, virtually atom-by-atom, to the required

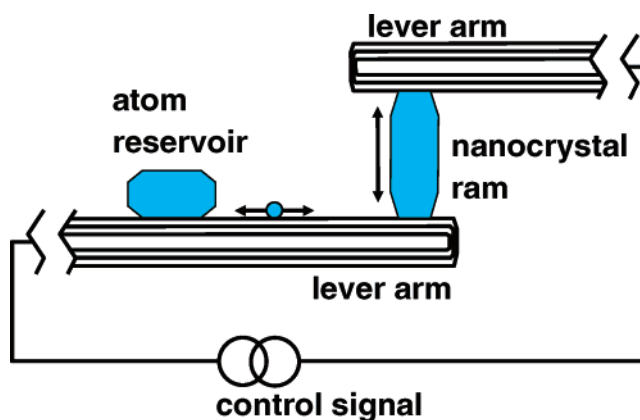


Figure 1. Schematic illustration of a linear nanomotor device. A nanocrystal ram is sandwiched between two MWNT lever arms. On one nanotube a metal particle serves as an atom reservoir that can source or sink atoms to or from the nanocrystal ram. The nanotube conveys the thermally excited atoms between the atom reservoir and ram.

length. This design exploits the recent discovery of a nanoscale mass conveyor mechanism whereby electrical currents driven through nanotubes transport metal atoms on the nanotube surface.⁴ Reversing the current direction reverses the direction of atom transport. In the experimentally realized motor described in detail below, we use indium as the prototype nanocrystal material.

Our linear nanomotor is constructed and operated inside a high-resolution transmission electron microscope (TEM) with a custom-built nanomanipulation stage. Raw materials for the nanomotor are first prepared *ex situ* by decorating arc-grown MWNTs with indium nanoparticles via thermal evaporation. The decorated MWNTs are then mounted on the nanomanipulation stage and inserted into the TEM, where the motor configuration of Figure 1 is created *in situ*. Using the nanomanipulator, two MWNT lever arms are placed in

* Corresponding author. E-mail: azettl@physics.berkeley.edu.

[†] Department of Physics, University of California at Berkeley.

[‡] Materials Sciences Division, Lawrence Berkeley National Laboratory.

[§] Center of Integrated Nanomechanical Systems, University of California at Berkeley.

^{||} Department of Materials Science and Engineering, University of California at Berkeley.

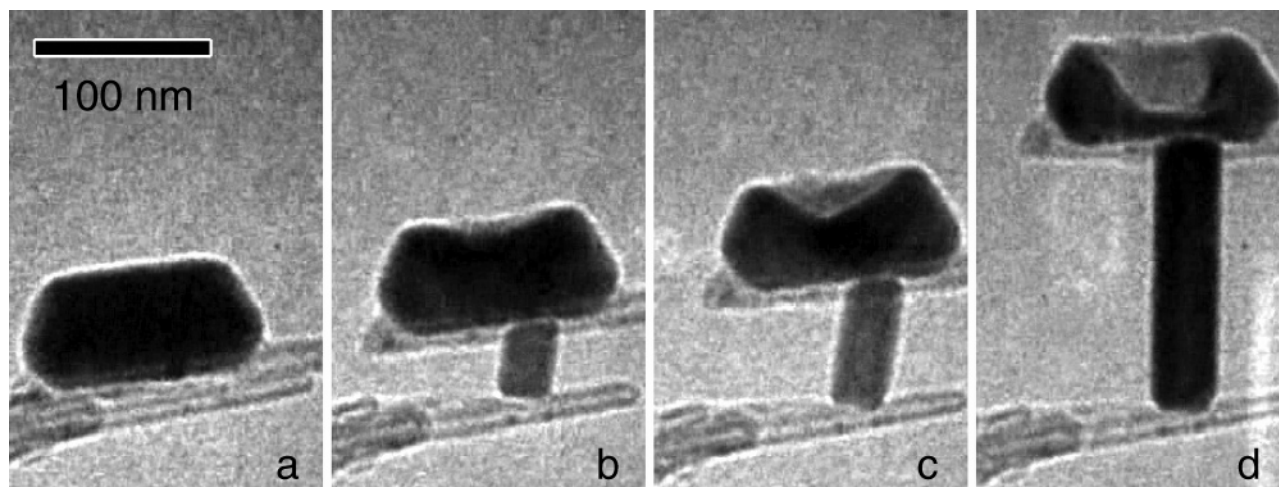


Figure 2. A time series of TEM video images spanning 60 s showing nanocrystal ram extension. (a) Two MWNTs lie in contact with one another. A reservoir of indium atoms rests on the top nanotube. (b) Driving $2.1 \mu\text{A}$ through the circuit creates the nanocrystal ram, which begins to push the MWNTs apart. The material for the growing crystal comes from the atom reservoir, which now shows a small dip. (c) The nanocrystal ram has grown to $\sim 75 \text{ nm}$ long, and the dip in the atom reservoir is more prominent. (d) At full extension the nanocrystal ram is more than 150 nm long. The bright reflections to the lower right and upper left of the ram indicate that the ram consists of a single crystal domain.

an overlapping parallel arrangement with an indium nanoparticle present near the overlap junction to serve as the atom reservoir. By applying a voltage across the MWNT lever arm junction with external electronics, an electrical current is established through the lever arms and the junction.

The completed device operates by using the MWNT lever arms as tracks for thermally activated, electrically directed indium surface diffusion.⁴ Indium atoms from the atom reservoir are transported to the junction region, where a single indium nanocrystal ram is grown directly between the lever arms. As the nanocrystal ram grows in length, it pushes the two MWNT lever arms apart. The ram growth rate and final length are fully controlled by the voltage applied to the lever arms. Importantly, the ram extension process is reversible, allowing cyclical motor operation.

The time series of TEM video images in Figure 2 clearly shows the ram extension mode of operation. Initially (Figure 2a) no nanocrystal ram is present and the parallel MWNT lever arms are in direct contact. The prominent dark indium nanocrystal visible on the upper MWNT lever arm is the atom reservoir. When a current of $2.1 \mu\text{A}$ is driven through the MWNT lever arms, a nanocrystal ram begins to grow in the MWNT junction. In Figure 2b the ram has grown sufficiently to separate the lever arms by approximately 32 nm , and the atom reservoir shows a cavity in its upper surface. As the ram grows in length, the cavity in the reservoir becomes more prominent (Figure 2c). In Figure 2d, the ram length is over 150 nm , and the reservoir is nearly half depleted. Bright reflections from the nanocrystal ram, one of which is visible in the lower right-hand corner of Figure 2d, indicate that the nanocrystal ram consists of a single domain. A predetermined ram length can be achieved by reducing the drive voltage to zero at any time, which immediately quenches atom transport and locks in the nanocrystal ram geometry.

When the reservoir-containing lever arm is biased positively (i.e., when it constitutes the anode), the ram grows

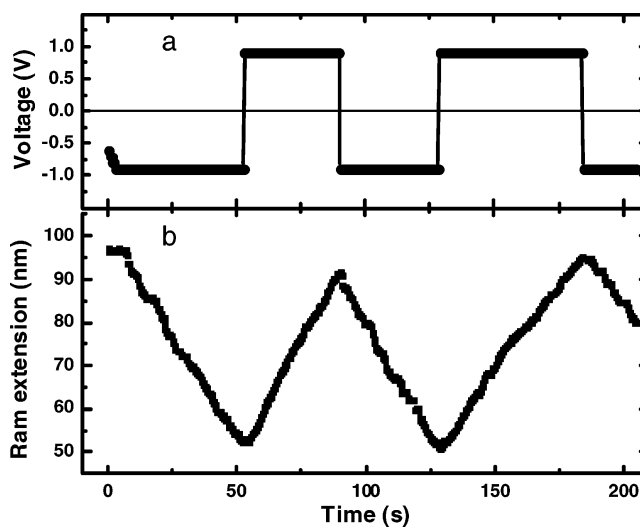


Figure 3. Controllable, reversible nanocrystal ram extension. The applied voltage (a) and ram extension length (b) are plotted versus time for a typical linear nanomotor device. Alternating the control voltage between 0.9 and -0.9 V causes the ram to grow and shrink linearly.

and the reservoir is depleted, as is shown in Figure 2. Reversing the voltage drives indium in the opposite direction, causing the ram to contract and the reservoir to refill. The extension/retraction process is repeatable, allowing cyclical linear motor operation. Figure 3 shows, for a different nanomotor of virtually identical design, details of this cyclical process. As the control voltage (upper panel) is switched sequentially between $+0.9$ and -0.9 V , the ram length grows and shrinks linearly with time, as shown in the lower panel of the Figure. The nanomotor is seen here to cycle regularly with a stroke of $\sim 45 \text{ nm}$ and a speed of $\sim 1 \text{ nm/s}$. Increasing (decreasing) the drive voltage increases (decreases) this rate. At low drive voltages, the (thermally activated) atom transport dramatically slows as the Joule heating is reduced. The drive voltage upper limit, and hence maximum speed,

is fixed by the requirement that the nanocrystal remains below its melting point. Even after repeated motor cycling, the reservoir is replenished at the end of each contraction cycle, indicating that indium loss mechanisms, such as evaporation or diffusion off the MWNT lever arms, are negligible during normal motor operation.

Nanocrystals tend to be perfect, single crystals,⁵ so it is not surprising that it is possible to grow a single crystal of indium at these length scales. The final crystal is clearly far from the thermodynamic equilibrium shape suggested by the Wulff construction, implying a growth mode dominated by kinetics. Atoms only reach the engine nanocrystal through surface diffusion; gas-phase transport is negligible because of indium's low vapor pressure. Thus, the growth direction may be determined largely by the interfacial plane between the crystal and the nanotube. (By analogy with indium on graphite we expect this to be the {111} plane.) For facets larger than a few tens of nanometers, the energy barriers for the nucleation of shape changes are large enough to prevent a nonequilibrium crystal from reverting spontaneously to a lower energy state.⁶ Thus, there is little intrinsic limitation on the types of crystal morphologies (e.g., aspect ratios) that can be achieved with proper management of this type of directed surface transport.

The nanocrystal motor has important qualitative advantages over other small-scale synthetic actuators. It does not suffer the friction problems of microelectromechanical systems such as comb drives, nor does it have the inherently tiny stroke typical of deformable mechanisms made of piezoelectric or bimorph materials. This design is a model of spatial efficiency, effectively incorporating typical (macroscopic) linear motor components of piston, cylinder, and valves into a single homogeneous nanocrystal. Excepting the atom reservoir, whose volume is dictated only by the intended application of the motor, the largest spatial dimension of the motor is equal to the nanocrystal ram stroke. Relative to piezoelectric and electrostatic actuators, our nanomotor also operates at very low voltage. Furthermore, its intrinsic "set and forget" feature allows the motor to indefinitely maintain any given displacement within its range of motion with zero power consumption, which may be advantageous in some applications.

A complete thermodynamic description of the nanocrystal growth process must account for the flow of heat, mass, and charge. The well-studied phenomenon of frost heaving provides a surprisingly close analogy. Contrary to the naïve expectation, frost heaving, or the upward growth of ice crystals in porous soils, is not driven by the volume expansion of water upon freezing.^{7,8} Rather, unfrozen water, stabilized below the bulk freezing temperature by curvature, surface, or solute effects, is drawn toward the freezing front by a gradient in the chemical potential.⁹ The resulting pressures can do work against, for example, a gravitational potential, even as heat is removed from the system.¹⁰ In the simplest geometries, the maximum crystallization pressure, P_{\max} , is given by $P_{\max} = \rho L(T_m - T)/T_m$, where ρ is the density of ice, L is the enthalpy of fusion, T is the temperature

of the fluid at the freezing front and T_m is the bulk freezing temperature.¹¹

In the case presented here, indium is driven toward the growth site by an electric field-induced chemical potential gradient. We propose that premelting at the nanotube/indium crystal interface drives the growth of the indium crystal against the applied mechanical pressure, in the same way that interfacial premelting drives frost heave.⁹ Surface melting on indium microcrystals has been observed as much as 36 K below the bulk melting temperature,¹² and interaction with the graphene surface of the nanotube may further lower the premelting onset temperature.^{13–15}

The frost heave analogy allows the examination of the available force and volumetric power density of the nanocrystal ram motor. Taking L equal to the latent heat of fusion of liquid indium (0.034 eV/atom¹⁶), and the reduced temperature $(T_m - T)/T_m = 10^{-2}$, we get an available ram pressure of $P_{\max} = 20$ bar. Assuming a ram cross-sectional area of $(36 \text{ nm})^2$, the associated force $F_r = 2.6$ nN. This may be a lower limit because both the electrostatic pressure imparted to the indium atoms by the control voltage and the adsorbed gas-to-liquid condensation energy favor ram growth. (Of course the strength of the ram, although likely much greater than that of bulk, polycrystalline indium, imposes an independent limit on its force capabilities.) As a check, we calculate the force needed to pry the MWNT lever arms apart in the configuration of Figure 2. Modeling the lever arms as cantilevered beams, the standard Euler–Bernoulli beam deflection expression¹⁷ $F = 3 E I d / l^3$ relates the transverse force, F , applied to the free end of the beam to the beam's Young's modulus, E , cross-sectional areal moment of inertia about its central axis, $I = \pi (r_{\text{outer}}^4 - r_{\text{inner}}^4) / 4$, displacement from equilibrium, d , and length, l . With $E \approx 1$ TPa,¹⁸ $r_{\text{outer}} = 16$ nm, $r_{\text{inner}} = 6$ nm, $l = 3$ μm , and $d = 140$ nm, we find $F \approx 1$ nN, within the available motor force capability determined above (possible electrostatic forces between the lever arms are substantially smaller). Linear nanoscale biomotors are much less forceful, typically operating in the piconewton range.¹⁹

In terms of volumetric power density, the nanocrystal ram compares favorably with competing motor technologies. We have observed nanocrystal ram extension velocities in excess of 1900 nm/sec, where the measurement was limited by the TEM video update rate of 30 frames per second. This velocity, together with the ram force, F_r , implies a motor power output capability of 5 fW. The available power density, Π_a , varies inversely with ram extension. For the motor shown in Figure 2, Π_a is initially (assuming a single monolayer nanocrystal) ~ 8 GW/m³ and decreases to 20 MW/m³ at ram full extension. In comparison, typical biomotors^{19–21} achieve power densities of less than 30 MW/m³, whereas the power density of a refined macroscopic linear internal combustion engine is around 50 MW/m³ (calculated for a 2004 Toyota Camry 210 hp V6, where the 3-L displacement has been taken as the working volume). The power density comparison with biomotors is somewhat surprising, given that the chemical reactions driving biomotors are typically an order of magnitude larger than the per-atom latent heat

of fusion of indium; this again highlights the spatial efficiency of our nanocrystal motor. If macroscopic force output is desired, these nanoscale linear motors could be ganged, as in the case where molecular biomotors combine to form muscle tissue.

The indium nanocrystal-powered motor is ideal for radiation-resistant, vacuum-compatible actuation, but with appropriate choice of materials this general process could be tailored for other practical applications. In this simplest nanomotor configuration, both the requisite heating and electric field are derived from a single electrical supply, which supplies power in the microwatt range to the device. Nearly all of this power goes to heat, but if necessary the nanomotor's efficiency could be enhanced by using a ram material that was mobile at ambient temperatures. Crystal growth is known to occur in environments ranging from vacuum to in vivo.²² We have fabricated rams composed of indium and cobalt, but beyond metals there is a wide class of materials known to electrocrystallize, including calcium carbonate²³ and organic conductors.²⁴ For coupling the motor to a surrounding mechanism, carbon nanotubes may be preferred even in other applications because they are chemically inert, have a high-aspect ratio, and are the stiffest known material.

From a thermodynamic standpoint, our linear nanocrystal-powered motor is unusual in that it does work while converting the working fluid to the low energy phase. In contrast, the steam engine, for example, drives an energetically expensive phase transition and then extracts work from the resulting gas. In the nanocrystal nanomotor case, the phase transition is exothermic and drives the actuator directly. The precise, responsive control afforded by electrically directed atomic transport harnesses these typically high energy densities to drive a compact, powerful motor.

Acknowledgment. This work was supported in part by the National Science Foundation and the U.S. Department of Energy.

References

- (1) Fuhrer, M. S.; Nygard, J.; Shih, L.; Forero, M.; Yoon, Y. G.; Mazzone, M. S. C.; Choi, H. J.; Ihm, J.; Louie, S. G.; Zettl, A.; McEuen, P. L. *Science* **2000**, *288*, 494–497.
- (2) Hisamoto, D.; Lee, W. C.; Kedzierski, J.; Takeuchi, H.; Asano, K.; Kuo, C.; Anderson, E.; King, T. J.; Bokor, J.; Hu, C. M. *IEEE Trans. Electron Devices* **2000**, *47*, 2320–2325.
- (3) Judy, J. W. *Smart Mater. Struct.* **2001**, *10*, 1115–1134.
- (4) Regan, B. C.; Aloni, S.; Ritchie, R. O.; Dahmen, U.; Zettl, A. *Nature* **2004**, *428*, 924–927.
- (5) Chen, C. C.; Herhold, A. B.; Johnson, C. S.; Alivisatos, A. P. *Science* **1997**, *276*, 398–401.
- (6) Rohrer, G. S.; Rohrer, C. L.; Mullins, W. W. *J. Am. Ceram. Soc.* **2001**, *84*, 2099–2104.
- (7) Henry, K. S. *U.S. Army Corps of Engineers, Cold Regions Research and Engineering Laboratory*; Technical Report 00-16, 2000; 1–19.
- (8) Taber, S. *J. Geol.* **1929**, *37*, 428–461.
- (9) Rempel, A. W.; Wettlaufer, J. S.; Worster, M. G. *J. Fluid Mech.* **2004**, *498*, 227–244.
- (10) Ozawa, H. *Phys. Rev. E* **1997**, *56*, 2811–2816.
- (11) Derjaguin, B. V.; Churaev, N. V. *J. Colloid Interface Sci.* **1978**, *67*, 391–396.
- (12) Pavlovskaya, A.; Dobrev, D.; Bauer, E. *Surf. Sci.* **1994**, *314*, 341–352.
- (13) Dash, J. G. *Science* **1989**, *246*, 1591–1593.
- (14) Wilen, L. A.; Wettlaufer, J. S.; Elbaum, M.; Schick, M. *Phys. Rev. B* **1995**, *52*, 12426–12433.
- (15) Wilen, L. A.; Dash, J. G. *Phys. Rev. Lett.* **1995**, *74*, 5076–5079.
- (16) Lide, D. R. *CRC Handbook of Chemistry and Physics*, electronic ed.; CRC Press: Boca Raton, FL, 2000.
- (17) Ruoff, R. S.; Lorents, D. C. *Carbon* **1995**, *33*, 925–930.
- (18) Poncharal, P.; Wang, Z. L.; Ugarte, D.; De Heer, W. A. *Science* **1999**, *283*, 1513–1516.
- (19) Visscher, K.; Schnitzer, M. J.; Block, S. M. *Nature* **1999**, *400*, 184–189.
- (20) Soong, R. K.; Bachand, G. D.; Neves, H. P.; Olkhovets, A. G.; Craighead, H. G.; Montemagno, C. D. *Science* **2000**, *290*, 1555–1558.
- (21) Limberis, L.; Stewart, R. J. *Nanotechnology* **2000**, *11*, 47–51.
- (22) Aizenberg, J. *Adv. Mater.* **2004**, *16*, 1295–1302.
- (23) Rinat, J.; Korin, E.; Soifer, L.; Bettelheim, A. *J. Electroanal. Chem.* **2005**, *575*, 195–202.
- (24) Hillier, A. C.; Ward, M. D. *Science* **1994**, *263*, 1261–1264.

NL0510659